

Comparative Simulation Study of GNR-FETs using EHT- and TB-based NEGF

Ming Zhang, Qiushi Ran, Ximeng Guan, Jinyu Zhang, Yan Wang, and Zhiping Yu

Institute of Microelectronics, Tsinghua University

Beijing 100084, China

Tel: +86-10-6278-4684 ext. 123, Fax: +86-10-6277-1130, Email: m-zhang03@mails.tsinghua.edu.cn

Abstract—A comparative study of graphene nanoribbon MOSFET (GNR-FET) using the extended Hückel theory (EHT) and tight-binding (TB) is conducted within the frame of the self-consistent ballistic non-equilibrium Green's function (NEGF) formalism. The bandgap variation in armchair-edged GNR (aGNR) induced by the length of the edge bond, as well as the transport characteristics with bond length relaxation, is studied in this paper. A strong structural dependence of aGNR-FET performance on the bond length is also observed and discussed.

Keywords- graphene nanoribbon; NEGF; EHT

I. INTRODUCTION

Graphene nanoribbon MOSFET (GNR-FET) is a promising device structure for CMOS-plus era because of the ultimately-thin channel thickness (mono-atomic layer) and high hole and electron mobilities [1][2]. However, it has become apparent recently that the gate controllability of GNR-FETs is very sensitive to the ribbon (i.e., channel) width and orientation [3] because the property of GNR can vary from metallic to semiconductive. By contrast, the experimental results show that narrow GNRs ($2\text{nm} \pm 0.5\text{nm}$), rather than the wide ones, still preserve a proper bandgap for MOSFET [4] as predicted for the armchair-edged GNR due to the edge bond relaxation [5]. In this paper, we compare both the bandgap yielded by the extended Hückel theory (EHT) and tight-binding (TB) methods due to the edge bond relaxation [5]. The ballistic non-equilibrium Green's function (NEGF) quantum transport computation is conducted based on both methods to study the performance of armchair-edged GNR-FETs (aGNR-FET) (See Fig.1). The simulation is implemented self-consistently with 3D Poisson's equation. The computation efficiency of both methods is comparable, while EHT is capable of modeling impacts of ribbon-edge termination and structural relaxation in a more direct physical way. The merits of EHT allow us to look into the influence of bond relaxation on the transport characteristics of aGNR-FET which leads to significant variations in I - V performance.

II. SIMULATION SCHEME

A. The Extended Hückel Theory

Accurate calculation of electronic structure and atomistic-level simulation of device performance, including a large number of atoms still represent a major challenge in the device modeling and simulation, mainly due to their high computational demand. Despite of recent progress of highly

efficient *ab initio*, the density-function-theory (DFT) is still computationally prohibitive in applying to systems with more than 200 atoms. Alternatively, the semi-empirical extend Hückel theory (EHT) provides a good tradeoff in between accuracy and efficiency [6]. By taking an explicit form of atomic orbitals, EHT can also provide more freedom than tight-binding (TB) to deal with bandstructure changes induced by bond relaxation, making it appealing for novel material modeling. Unlike TB, EHT provides the capability of simulating different types of atoms within the similar sets of parameters [7][8]. The overlapping matrix used in EHT can be calculated in advance with little effort by a variety of integration techniques [9], and the method offers more insight into the physical property of the device performance.

Within the EHT, the Slater type orbitals (STOs), a non-orthogonal atomic orbital basis set, are chosen for each atom, whose explicit form can be found in [9]. A parameterized double ζ wavefunction [10] (TABLE I. [11]) is adopted to calculate the overlapping matrix and the Hamiltonian. The matrix elements of the Hamiltonian are evaluated as

$$\begin{aligned} H_{ii} &= E_i \\ H_{ij} &= \frac{1}{2} K_{EHT} (E_i + E_j) S_{ij} \quad (i \neq j) \end{aligned} \quad (1)$$

where $K_{EHT}=2.8$ for carbon, and E_i and E_j are the on-site energies and element of the overlapping matrix S_{ij} is calculated by the following integration with techniques discussed [9]

$$S_{ij} = \int \varphi_i^*(\mathbf{r}) \varphi_j(\mathbf{r}) d^3 \mathbf{r} \quad (2)$$

where φ_i and φ_j are basis functions in STO form for atoms. Thus the impact of bond length variation will be included in the overlapping matrix, which further results in the corresponding changes in Hamiltonian.

TABLE I. PARAMETERS FOR CARBON IN EXTENDED HÜCKEL THEORY

Orbital	E_{onsite}	C_1	C_2	ζ_1	ζ_2
2s	-20.316	0.741		2.037	
2p	-13.670	0.640	0.412	1.777	3.249

By using the linear combination of atomic orbitals (LCAO), we can achieve the bandstructure by solving the generalized eigenvalue problem [12]

$$H(k)\psi(k) = E(k)S(k)\psi(k) \quad (3)$$

where the Hamiltonian and overlapping matrix are expressed in the form of the Bloch sum of orbital basis, which indicates

$$H_{ij}(k) = \sum_{j'} e^{ikR_{j'}} H_{ij'}, \quad (4)$$

$$S_{ij}(k) = \sum_{j'} e^{ikR_{j'}} S_{ij'}$$

Here subscript j' runs over all the orbitals equivalent to the orbital j , and $R_{j'}$ denotes the vector pointing from j to j' .

B. Transport Modeling and Simulation

Based on both EHT and TB model, an aGNR-FET (Fig.1) is simulated using ballistic NEGF in our transport simulation, which treats the system with open boundary conditions by the surface green functions $g_{s,d}$ of the source and drain regions, calculated through a highly convergent iteration scheme [13]. The retarded Green's function in the device region is calculated [14] by

$$G^r = \left[(E + iz^+)S - H - U - \Sigma_S - \Sigma_D \right]^{-1} \quad (5)$$

where S is the overlapping matrix, H for the Hamiltonian of GNR in the simulated region, U for the potential energy, and Σ_S and Σ_D are the self-energy matrices for the source and drain regions. The potential energy is calculated by the 3D Poisson's equation with floating boundary condition of two contacts in a hexagonal mesh. The gate voltage is included through the fixed boundary condition on both the top and back gates. The results are derived by solving Poisson's equation and NEGF iteratively until self-consistency is achieved. Though the potential energy U should be modified by the overlapping

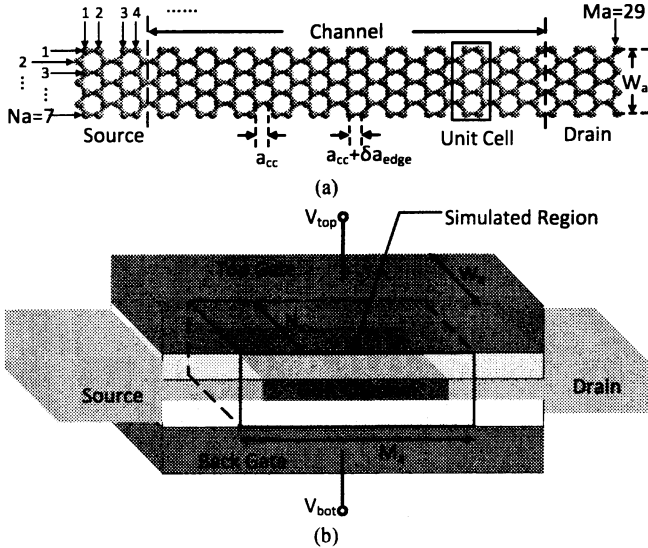


Fig. 1 (a) The armchair GNR structure. We choose $N_a = 7$ and $M_a = 29$ GNR as the simulated region. (b) The DG structure of the simulated device. The Fermi level is set to -12.3 eV at drain and source while the one of intrinsic GNR is -13.0 eV.[10] The effective oxide thickness is set to 0.5 nm.

matrix S in principle, we use U directly since S is close to the identity matrix I . To improve the computational efficiency, an iterative inversion method is adopted [15], in addition to the contour integration in energy space of numerical quadrature [16]. The current is calculated through the Landauer-Büttiker formalism [14], which expresses the current by integrating transmission weighed by the Fermi-Dirac distribution.

$$I_{DS} = \frac{2}{\hbar} \int T(E)(f_S - f_D) dE \quad (6)$$

$$= \frac{2}{\hbar} \int Tr \left(\Gamma_S G^r \Gamma_D (G^r)^\dagger \right) (f_S - f_D) dE$$

where $T(E)$ denotes the transmission, $\Gamma_{S,D} = i(\Sigma_{S,D} - \Sigma_{S,D}^\dagger)$ and f_S, f_D denote the Fermi-Dirac distribution in the source and drain end.

Since substitution of atoms on the ribbon edges [17] will lead to the doping effect of GNR, we simply neglect the doping details and assume that both source and drain extensions of the GNR are in thermal equilibrium with metal contacts, and thus having the fixed (i.e., applied) Fermi levels. This simplification assumes the fast momentum relaxation in source/drain region, which is required by a good contact to minimize the voltage drop inside the drain/source area.

III. RESULTS AND DISCUSSIONS

We have investigated how the width of the armchair GNR and edge bond relaxation affect the bandgap in electronic structure. In our calculations, bond length is weakly dependent upon N_a (See Fig.1 for definition), and the C-C bonds along the channel at two edges of the ribbon are shortened by approximately 3.4% [5].

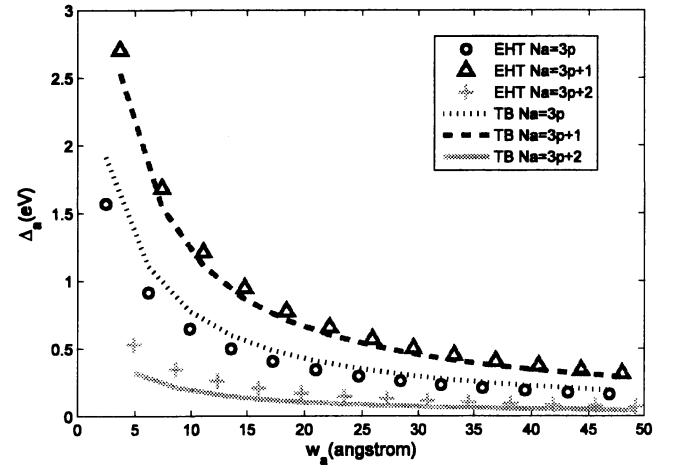


Fig. 2 The bandgap Δ_a vs. ribbon width w_a with the number of atoms N_a (defined in Fig. 1) as parameter. TB and EHT results share a common trend in the bandgap, but differ slightly in value. See [5] for the TB parameter. a_{cc} equals $1.424, 1.422$ and 1.423 Å, respectively for $N_a = 3p, 3p+1$, and $3p+2$, with p the positive integer.

Our result (Fig. 2) is similar to that from the TB and first-principle calculations. The figure shows the result yielded by using EHT and calibrated TB parameters proposed in [5].

However, EHT does not need fitting parameters while TB does[8], especially for systems whose physical properties are strongly affected by the geometry, while the computational cost is acceptable. The result of either methods shows the same trends that the bandgaps diminish when the widths of the graphene ribbon grow, thus making the wide GNR-FET lack of gate controllability[4]

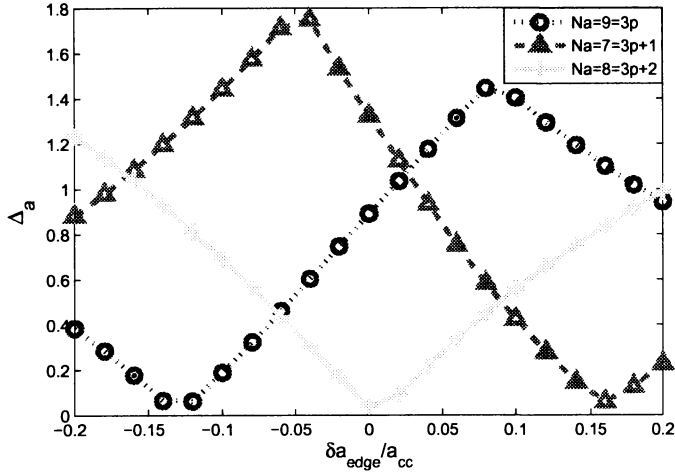


Fig. 3 The bandgap Δ_a variation with the length of edge bonds at different N_a of armchair GNR. Note that the relaxed bond length due to the hydrogen passivation corresponds to $\delta a_{edge} / a_{cc} \approx -0.034$. [5]

Fig. 3 shows how bandgaps at different N_a vary with the bond length at edges, which may result from the passivation of edged carbon atoms. In sharp contrast to wide GNRs, the results show that all of the three types of narrow aGNRs can become semiconductive under the edge bond length perturbation, which indicates the sensitivity to gate voltage.

Since the electronic structure of armchair GNR has a quantized width-dependence [3] (which is weakened by the edge bond relaxation), GNR with $N_a=3p+1$ (where p is a positive integer) will provide good performance. We choose the $N_a=7$ and $M_a=29$ aGNR structure shown in Fig.1 as the simulated region, whose left and right sides are regarded as source/drain areas with fixed Fermi level due to the doping effect.

A comparison of transport characteristics simulated using the EHT-based and TB-based NEGF is shown in Figs. 4-5. Bond length relaxation of GNR is taken into account in the EHT calculation, which has a significant influence on the transport. Fig. 4 shows the output characteristics simulated under different top gate voltage V_{top} with $V_{bot}=0V$. A stronger short-channel effect in EHT simulation is observed, compared to TB, as well as an exceedingly high drain current in the saturation region with $a_{cc}=1.44\text{\AA}$, while the drain current of $a_{cc}=1.42\text{\AA}$ remains almost the same as the one yielded through TB. From Figs.4, it is not hard to infer that GNR-FET will show a larger I_{ON} current under a tensile stress.

Fig. 5 plots the drain current I_{DS} under the symmetry gate voltage operation ($V_{top}=V_{bot}$) for all the EHT and TB results. A much larger subthreshold current appears in EHT simulation in

the case of $a_{cc}=1.44\text{\AA}$ compared to the result of $a_{cc}=1.42\text{\AA}$, which is similar to that of TB. Moreover, the case of $a_{cc}=1.42\text{\AA}$ exhibits a larger subthreshold slope than the one of $a_{cc}=1.44\text{\AA}$

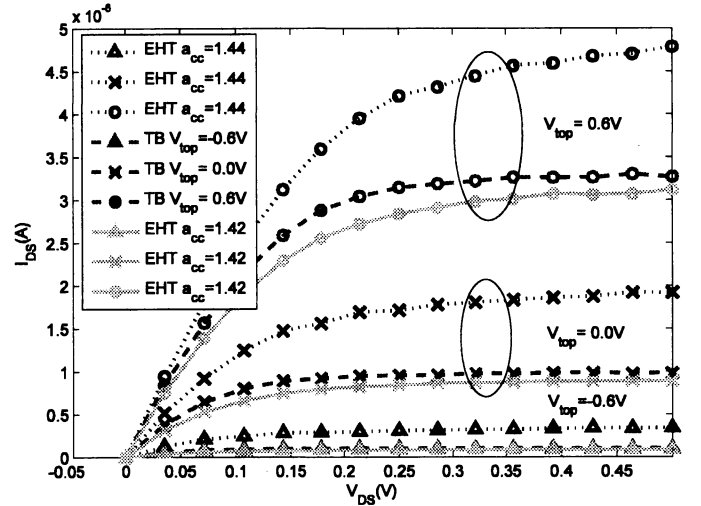


Fig. 4 The simulated I_{DS} - V_{DS} curves plotted with different marks regarding different V_{top} with $V_{bot}=0V$. TB results are shown by the dashed lines, EHT results with $a_{cc}=1.42\text{\AA}$ by the solid lines and $a_{cc}=1.44\text{\AA}$ by the dotted lines.

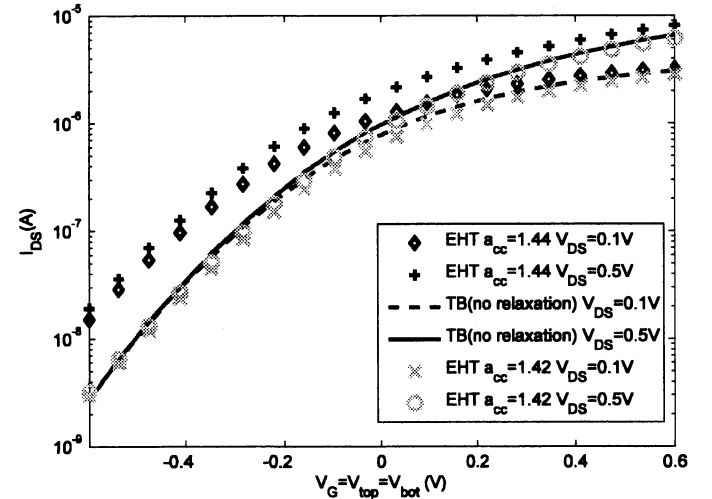


Fig. 5 The drain current versus gate voltage under different bias voltages derived by different methods. The TB results are shown in solid line and dashed line. The EHT results are plotted under different marks. An large subthreshold current is observed in EHT result when $a_{cc}=1.44\text{\AA}$ while the TB curve maintain similar to the one of $a_{cc}=1.42\text{\AA}$, which exhibits a larger subthreshold slope.

The difference among three cases based on EHT and TB methods can be explained by the transmission shown in Fig. 6, as the current can be derived from the integration of the transmission weighed by Fermi-Dirac distribution. It exhibits the transmissions of the GNR channel in three cases under a bias of $V_{DS}=0.5V$ with $V_{top}=0.6V$ and $V_{bot}=0V$. Since multiplied by $(f_S - f_D)$ in the integral, the transmission between the Fermi levels of the drain and source (E_{FS} and E_{FD}) has the most contribution to the current, which is downward shifted

relatively in the case of $a_{CC}=1.44\text{\AA}$, illustrating the reason for high I_{ON} current and low subthreshold slope. The downward shift can be interpreted by the presumption that the increase of bond length reduces the coupling of the orbitals (i.e. overlapping matrix elements), thus narrowing the bandgap, which eventually shifts the transmission in the case of $a_{CC}=1.44\text{\AA}$. EHT-based simulation, standing on more basic physics than TB-based one, has the capability to reflect the

ACKNOWLEDGMENT

The authors sincerely appreciate the discussion on the calculation of EHT via e-mails with J. Cerdá from Instituto de Ciencia de Materiales, Madrid, Spain. This work is supported by grants from NSF (\#90307016) and from Ministry of Science and Technology (\#2006CB302700), both in China.

REFERENCES

- [1] M. C. Lemme, T. J. Echtermeyer, M. Baus, and H. Kurz, "A graphene field-effect device," IEEE EDL, vol. 28, pp. 282–284, April 2007.
- [2] B. Obradovic, R. Kotlyar, F. Heinz, P. Matagne, T. Rakshit, D. Nikonov, and M. A. Stettler, "Carbon nanoribbons: an alternative to carbon nanotubes," SISPAD Proceedings, pp. 27–30, Sept. 2006.
- [3] X. Guan, M. Zhang, Q. Liu, and Z. Yu, "Simulation Investigation of Double-Gate CNR-MOSFETs with a Fully Self-Consistent NEGF and TB Method," IEDM Proceedings, pp. 761, 2007.
- [4] X. Wang, *et al.*, "Room-Temperature All-Semiconducting Sub-10-nm Graphene Nanoribbon Field-Effect Transistors," Phys. Rev. Lett., vol. 100, pp. 206803.1–206803.4, May 2008.
- [5] Y. W. Song, M. L. Cohen, and S. G. Louie, "Energy Gaps in Graphene Nanoribbons," Phys. Rev. Lett., vol. 97, 216803.1–216803.4, 2006.
- [6] D. Kienle, J. I. Cerdá, A. W. Ghosh, "Extended Hückel theory for band structure, chemistry, and transport. I. Carbon nanotubes," J. Appl. Phys. vol. 100, pp. 043714.1–043714.9, 2006
- [7] X. Guan, Q. Ran, M. Zhang, Z. Yu, and H.-S. Philip Wong, "Modeling of Schottky and Ohmic Contacts between Metal and Graphene Nanoribbons using Extended Hückel Theory-Based NEGF Method," unpublished.
- [8] D. Porezag, Th. Frauenheim, and Th. Köhler, "Construction of tight-binding-like potentials on the basis of density-functional theory: Application to carbon," Phys. Rev. B, vol. 51, p. 12947, 1995
- [9] H. Tai, "Generation of a two-center overlap integral over Slater orbitals of higher principal quantum numbers," Phys. Rev. A, vol. 45, no. 3, pp. 1454–1464, Feb 1992.
- [10] J. Cerdá and F. Soria "Accurate and transferable extended Hückel-type tight-binding parameters," Phys. Rev. B, vol. 61, no.12, pp. 7965, March 2000.
- [11] J. Cerdá, <http://www.icmm.csic.es/jcerda/index.html>
- [12] H. Raza, E. C. Kan, "An extended Hückel theory based atomistic model for graphene nanoelectronics", J Comput Electron, DOI10.1007/s10825-008-0180-z, 2008.
- [13] M. P. L. Sancho, J. M. L. Sancho and J Rubio, "Highly convergent schemes for the calculation of bulk and surface Green functions," Phys. F: Met. Phys., vol. 15, pp. 851–858, 1985.
- [14] S. Datta, Quantum Transport: Atom to Transistor, Cambridge University Press, Cambridge, 2005
- [15] D. Nikonov, <http://www.nanohub.org/resources/1983/>, 2006
- [16] M. Brandbyge, J L Mozos, P. Ordejo, J. Taylor, and K. Stokbro, "Density-functional method for nonequilibrium electron transport," Phys. Rev B, vol. 65, 165401.1–165401.17, March 2002.
- [17] Q. Yan, *et al.*, "Intrinsic current-voltage characteristics of graphene nanoribbon transistors and effect of edge doping," Nano. Lett. vol. 7, pp. 1469–1464, 2007.

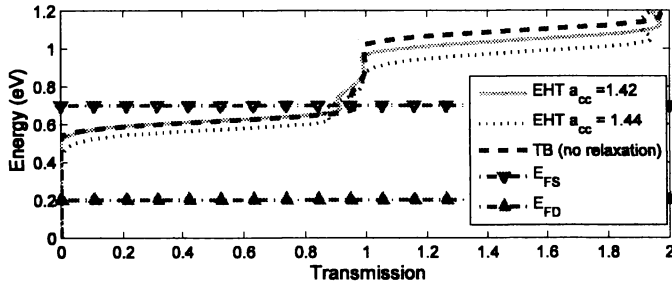


Fig. 6 The transmission given by TB and EHT of the two bond lengths under $V_{DS}=0.5V$, $V_{top}=0.6V$, $V_{bot}=0V$ (translated to the same E_{FS}). The curves of three cases are plotted in different type of lines. E_{FS} and E_{FD} , marked with upper and lower triangles, are the Fermi levels of source and drain ends. Transmission of EHT with $a_{CC}=1.44\text{\AA}$ (plotted in dotted line) is relatively downward shifted, leaving a larger integration within the interval between E_{FS} and E_{FD} than the one of other two cases.

performance variation due to the bond length relaxation. The performance of GNR devices under structural deformation can also be inferred from the results. The stress, which leads to a uniform tensile strain on the lattice, may probably contribute to a large I_{ON} current, but also to a significant subthreshold leakage current. On the other hand, a uniform compressive strain may improve the subthreshold slope and thus lower the subthreshold leakage, but in return, it may reduce I_{ON} current.

IV. CONCLUSION

Band structure variations derived by EHT and TB calculation due to the edged bond relaxation have been compared. EHT results of bandgap variation show that all armchair GNRs can reach the bandgap with a proper ribbon-edged bond length to achieve good gate controllability. A self-consistent EHT-based atomic-level NEGF simulation of an armchair DG GNR-FET coupled with 3D Poisson's equation is performed and compared with TB-based result. The transport characteristics of the devices illustrate a considerable sensitivity to structural variation. The EHT simulation offers a good insight into the transport of the armchair GNR-FETs under structural deformation and predicts the probable effect on I-V characteristics due to a uniform strain.